

Article

Synthesis, Mesomorphism and the Optical Properties of Alkyl-Deuterated Nematogenic 4-[(2,6-Difluorophenyl)ethynyl]biphenyls

Jakub Herman , Piotr Harmata , Michał Czerwiński , Olga Strzeżysz, Marta Pytlarczyk , Monika Zajac  and Przemysław Kula * 

Faculty of Advanced Technologies and Chemistry, Military University of Technology, 2 gen. S. Kaliskiego St., 00-908 Warsaw, Poland; jakub.herman@wat.edu.pl (J.H.); piotr.harmata@wat.edu.pl (P.H.); michal.czerwinski@wat.edu.pl (M.C.); olga.strzezysz@wat.edu.pl (O.S.); marta.pytlarczyk@wat.edu.pl (M.P.); monika.zajac@wat.edu.pl (M.Z.)

* Correspondence: przemyslaw.kula@wat.edu.pl

Abstract: The synthesis and characterization of new deuterated liquid crystal (LC) compounds based on phenyl tolane core is described in this paper. The work presents an alternative molecular approach to the conventional LC design. Correlations between molecular structure and mesomorphic and optical properties for compounds which are alkyl-hydrogen terminated and alkyl-deuterium, have been drawn. The compounds are characterized by mass spectrometry (electron ionization) analysis and infrared spectroscopy. They show enantiotropic nematic behavior in a broad temperature range, confirmed by a polarizing thermomicroscopy and differential scanning calorimetry. Detailed synthetic procedures are attached. Synthesized compounds show a significantly reduced absorption in the near-infrared (NIR) and medium-wavelength infrared (MWIR) radiation range, and stand as promising components of medium to highly birefringent liquid crystalline mixtures.

Keywords: infrared; flow chemistry; deuterium addition; nematic



Citation: Herman, J.; Harmata, P.; Czerwiński, M.; Strzeżysz, O.; Pytlarczyk, M.; Zajac, M.; Kula, P. Synthesis, Mesomorphism and the Optical Properties of Alkyl-Deuterated Nematogenic 4-[(2,6-Difluorophenyl)ethynyl]biphenyls. *Materials* **2021**, *14*, 4653. <https://doi.org/10.3390/ma14164653>

Academic Editor: Ingo Dierking

Received: 9 July 2021

Accepted: 14 August 2021

Published: 18 August 2021

Publisher's Note: MDPI stays neutral with regard to jurisdictional claims in published maps and institutional affiliations.



Copyright: © 2021 by the authors. Licensee MDPI, Basel, Switzerland. This article is an open access article distributed under the terms and conditions of the Creative Commons Attribution (CC BY) license (<https://creativecommons.org/licenses/by/4.0/>).

1. Introduction

Organic optical materials are used to construct many elements of optical devices operating in various spectral ranges, from ultraviolet [1–5] through visible [6,7] to infrared [8–13]. Most organic materials are passive elements; however, one group—mesomorphic materials—constitute the heart of active elements, where the wide tunable abilities of these materials are used. The near-infrared range (NIR), so important in fiber-optic communication, was not the main spectral area for which organic mesomorphic materials were developed. Instead, they were developed for the visible range and the entire display industry associated with it [14–21]. Therefore, all organic materials, especially mesomorphs, used in the near-infrared range, are not materials dedicated to this range. They show a number of disadvantages, such as parasitic absorption (the presence of absorption originating from overtones and combinational bands, primarily related to the vibration of C-H bonds in rings and alkyl chains) and indirectly related changes in optical signal depolarization [22–24]. Despite the fact that the absorption coefficients, related to higher than the first harmonic, have a lower level of magnitude, they still deteriorate the optical density of the liquid crystalline medium in NIR.

In order to reduce the absorption we decided to increase the weight of one of the most critical elements—hydrogen—by replacing the C-H bonds with C-D, which reduces the frequency of the fundamental vibration and shifts the absorption bands toward longer wavelengths [14,24–28]. The reduced mass causes such polyatomic systems, R-D or R-H, to be strongly affected, due to the high relative mass difference between protons and deuteriums. This in turn translates to the molecular vibration frequency shifts of fundamental

frequencies (3000 cm^{-1}) and higher harmonics (1700 nm) towards longer wavelengths, 2300 cm^{-1} and 2000 nm, respectively. This causes the optical density in important NIR window to be significantly lowered. Moreover, the deuteration of mesogenic molecules, as well as the fluorination, and/or chlorination approaches were proposed to shift the vibration bands beyond the spectrum of interest. The vibration bands of CF, CF₂ and CF₃ bonds occur at 7–9 μm . A modification of the fluorination solution is to propose the chlorination of liquid crystal molecules. This also allows for shifts of the vibration bands and overtones outside the area of interest [23,29–31]. Replacing fluorine with a heavier chlorine atom causes the C-Cl vibration wavelength to occur between approximately 12.5 and 15.4 μm [32]. While the intensity of the C-F overtones is relatively small, though still noticeable in the IR region, the overtone wavelength of C-Cl bonds is now longer than 6 μm , and therefore cleans up the window in the MWIR and LWIR regions. Nevertheless, the replacement of elastic aliphatic chains with short perfluorinated or chlorinated groups in liquid crystal molecules has a drastic effect on the presence of the mesophase. However, the liquid crystallinity decay problem for the fluorinated molecules is currently solved. There are many organic structures that exhibit temperature-wide nematic phases, even though they lack the flexibility and aspect ratio required previously.

The optical density of liquid crystal which is the active medium of many non-display optical devices is one of the key factors, either in high-power laser applications, [33,34] or in devices working at NIR and MWIR frequencies, especially those for which the working bands are close to C-H vibrations. High red shift observed for partially deuterated or perdeuterated materials can be exploited for enhancing the operating windows of “regular” nondeuterated liquid crystals. Dedicated materials for specific applications in the near-infrared range are the subject of our research. The possibility of extending the use of liquid crystals to NIR light could be very important in different areas, like optical fiber communications, with standard windows operating at 800–980 nm, 1300–1330 nm, and 1550–1670 nm, or in biomedical imaging, where the conventional therapeutical windows are centered at ranges of 650–950 nm (first window) or 1100–1350 nm (second window).

Liquid crystal devices can control the wavelength, polarization and phase, so they can be used to improve the performance of optical imaging systems even for biomedical applications, e.g., LC polarization controllers for bio-imaging, where LCs act as a simple variable retarder creating and controlling polarization changes [35–38]. LC-tunable filters were successfully demonstrated in research labs and some industrial environments to have a great potential in agriculture, process inspection, remote sensing and medical diagnosis for spectral and polarization imaging (SPI) and hyperspectral imaging (HSI). For those applications, the interest is usually in the near-infrared window (750–1300 nm), which is covered with LC devices, enhancing the functionality of optical imaging systems [39–44]. LCs can also be applied in optical systems based on a LCoS-SLM, that acts as a waveplate with a programmable spectra retardance function in the visible and NIR wavelength [45,46]. LCs can be applied to control the tuning of the metamaterial electromagnetic response in NIR in metamaterial–liquid crystal cell structures [20,47].

In this work we focused our attention around strongly nematogenic tolanses, from 4-[(2,6-difluorophenyl)ethynyl]biphenyls family—see Figure 1. Lateral fluoro-substitution, in particular a 2,6-difluorophenyl acetylene unit, offers unique and valuable nematic stability [48–52] together with increased birefringence. Although the structures itself are already known [50,51] we present a totally new, synthetic approach to the material which reflects the idea of reducing IR absorption by increasing the mass of the components of the molecule.

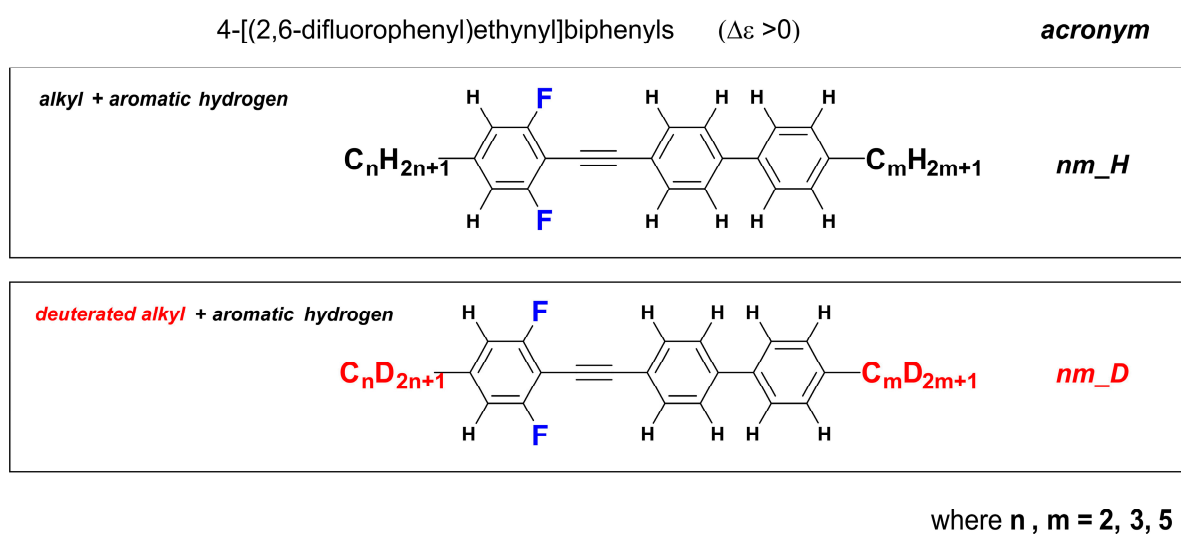


Figure 1. General structures of investigated materials.

2. Materials and Methods

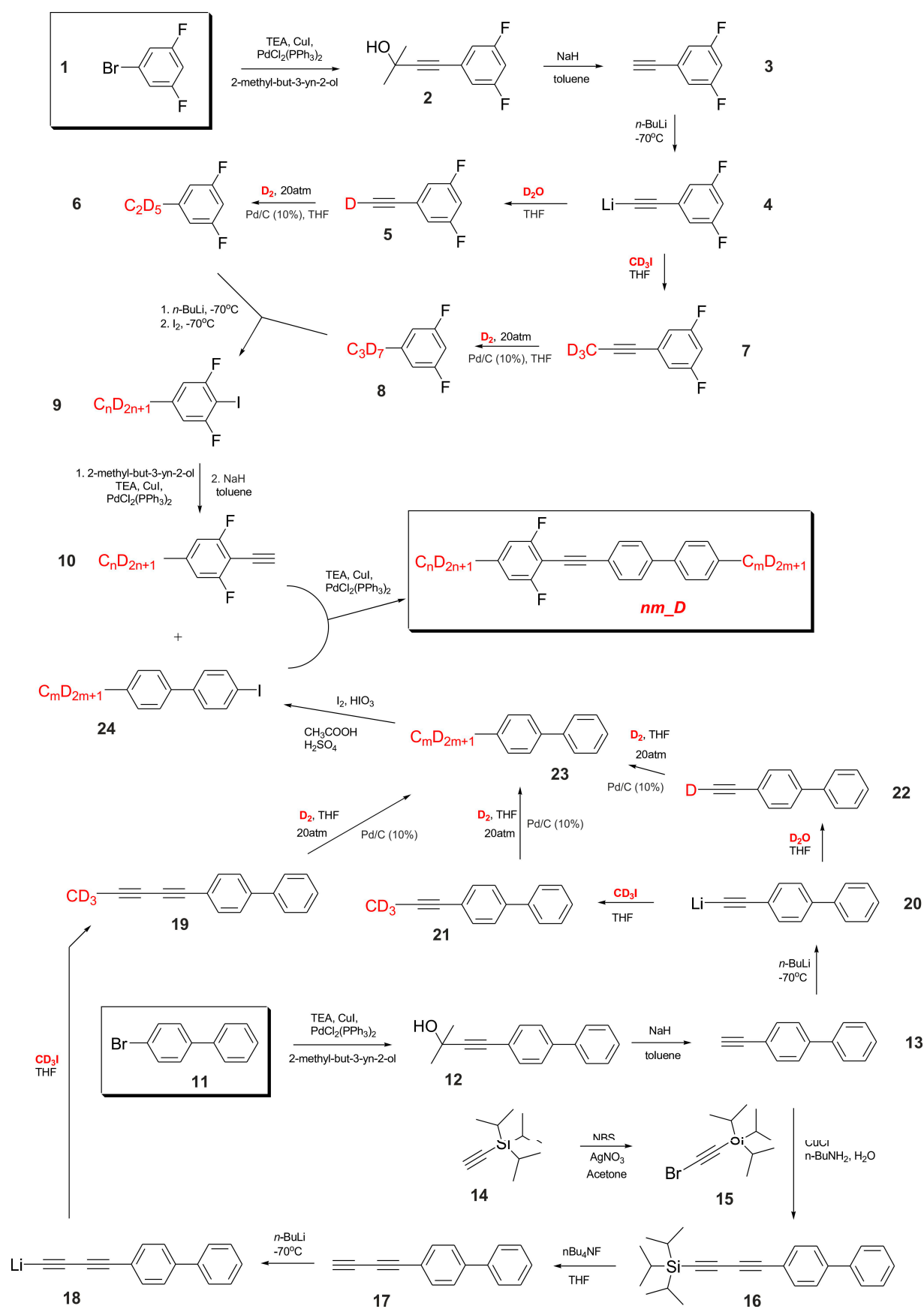
2.1. Materials

The genes 1-Bromo-3,5-difluorobenzene and 4-bromo-biphenyl[1,1'] were purchased from Fluorochem (Hadfield, UK) and used as received. The genes 1,8-diazabicyclo(5.4.0)undec-7-ene, and 2-methylbut-3-yn-2-ol were purchased from Acros Organics, (Geel, Belgium) and used as received. Toluene, acetone, hydrochloric acid, sodium nitrite, potassium iodide, anhydrous potassium carbonate and copper(I) iodide were purchased from Avantor Performance Materials Poland S.A (Gliwice, Poland) and used as received. Palladium(II) acetate, bis(triphenylphosphine)palladium(II) chloride, and sodium hydride (60% dispersion in mineral oil) were purchased from Sigma-Aldrich Sp.z.o.o (Poznan, Poland) and used as received. THF was distilled from sodium ketyl radical under nitrogen atmosphere prior to use. Methyl iodide- d_3 and heavy water D_2O were purchased from Armar AG (Dottingen, Switzerland).

The main source of deuterium we decided to use in this work was the deuterium gas D_2 , in situ generated during the electrolysis of heavy water, D_2O . The gas produced acted as a reactant in the palladium-catalyzed addition reactions to the carbon-carbon triple bond. A H-Cube Pro (ThalesNano, Budapest, Hungary) pressure flow reactor was used to carry out this process. Additionally, methyl iodide (d_3) was used as the deuterium source, which formed a chain with an odd number of carbon atoms in nucleophilic substitution reactions.

2.2. Synthesis

Synthetic process of alkyl-deuterated tolanses (with the acronym *nm_D*) began with 1-bromo-3,5-difluorobenzene **1**, which was coupled to a triple carbon-carbon bond, resulting 1-ethynyl-3,5-difluorobenzene **3**—see Figure 2. Then the proper lithium acetylide **4** was created and reacted either with heavy water, D_2O , or methyl iodide, d_3 —structure **5** and **7**, respectively. Both reacted with gaseous deuterium and formed the desired ethyl- d_5 **6** and propyl- d_7 **8** derivatives. Next ortho-directed metalation followed by iodination was performed **9**, and finally the Sonogashira coupling to a carbon-carbon triple bond, resulting in **10**. The right part of the tolane molecule was constructed using 4-bromobiphenyl **11** as a starting reagent and an analogous synthetic procedure. Additionally, we decided to create a pentyl- d_{13} homologue **23**, using the Cadiot-Chodkiewicz procedure for buta-1,3-diyne derivative **17**.

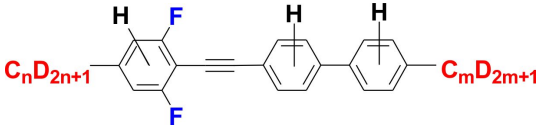
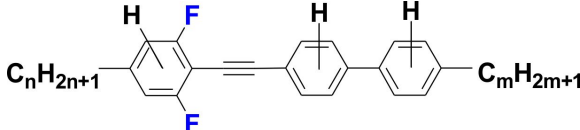
Figure 2. Synthesis of alkyl-deuterated tolans *nm_D*.

Finally, the tolanses *nm_D* were created using the Sonogashira protocol with 2-ethynyl-1,3-difluoro-5-alkylbenzene **10** and 4-alkyl-4'-iodo-[1,1']-biphenyl **24** as a substrates.

2.3. Mesomorphic Properties and Discussion

The sequence of phase transitions and their temperatures were determined by polarizing optical microscopy with the 'Olympus' BX51 polarizing microscope (Shinjuku, Tokyo, Japan), equipped with a Linkam hot stage THMS-600 (Linkam Scientific Instruments Ltd., Tadworth, UK) and by differential scanning calorimetry using the DSC SETARAM 141 instrument (KEP Technologies Group's DNA, Montauban, France) with the scanning rate 2 K min⁻¹ in both heating and cooling cycles. The phase situation of alkyl-deuterated structures *nm_D* was correlated with their hydrogen isotopologues *nm_H*—Table 1 and Figure 3. Differential scanning calorimetry graphs of investigated compounds were gathered in Supplementary Materials.

Table 1. Phase transition temperatures (°C) and enthalpies (kJ·mol⁻¹) from DSC measurements obtained during heating cycles.

Acronym	Phase Transition Temperatures [°C] (<i>Enthalpy</i> [kJ mol ⁻¹])	Temperature Range of Nematic Phase [°C]
<i>nm_D</i>		
22_D	Cr 107.2 (23.0) N 163.9 Iso	56.7
23_D	Cr 68.1 (17.5) N 174.8 Iso	106.7
32_D	Cr 73.2 (24.7) N 179.3 Iso	106.1
33_D	Cr 78.0 (26.6) N 186.8 Iso	108.8
25_D	Cr 72.0 (20.0) N 160.3 Iso	88.3
35_D	Cr 85.6 (24.8) N 170.3 Iso	84.7
<i>nm_H</i>		
22_H	Cr 108.9 (22.7) N 165.4 Iso	56.5
23_H	Cr 70.2 (18.8) N 173.8 Iso	103.6
32_H	Cr 74.7 (26.9) N 175.2 Iso	100.5
33_H	Cr 78.3 (26.9) N 186.5 Iso	108.2
25_H	Cr 73.6 (17.6) N 159.6 Iso	86.0
35_H	Cr 87.8 (24.1) N 169.7 Iso	81.9

Alkyl-deuterated structures showed similar nematic behavior compared to their hydrogen analogues; however, the temperature-wide nematic is seen for *nm_D* structures. This was due to the differences in crystalline–nematic transition temperatures, which were 1–3 °C lower, and nematic–isotropic liquid transitions temperatures, which were 1–3 °C higher for alkyl-deuterated structures. Correlation between enthalpies of melting was hard to extract, and there were no significant differences between investigated structures. Differential scanning calorimetry graphs of selected structures 23_H, 23_D and 35_H, 35_D are shown in Figure 3.

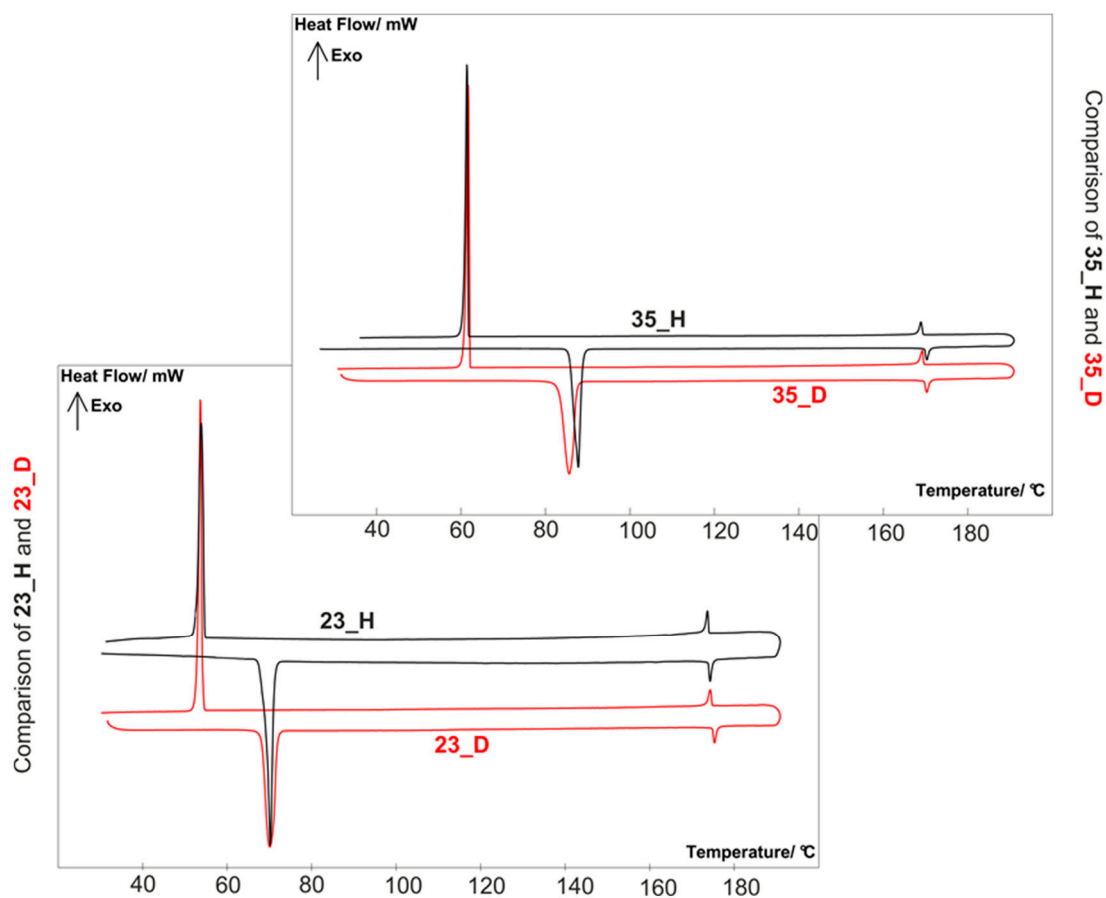


Figure 3. Comparison of DSC of selected hydrogen and deuterated structures.

2.4. Optical Properties and Discussion

Refractive indices of neat materials were measured by the Metricon Model 2010/M Prism Coupler (Metricon Corporation, Pennington, NJ, USA), equipped with 443 nm, 636 nm and 1550 nm lasers. Samples of liquid crystals were placed on glass plates rubbed with SE-130 polyimide (Nissan Chemical[®], Tokyo, Japan). Ordinary refractive index n_o and extraordinary refractive index n_e were measured separately using transverse-magnetic TM and transverse-electric TE polarization of incident beams. Samples were measured at elevated temperatures (5 Kelvin steps), with the limit of the setup at 200 °C. Exact values of refractive indices n_o , n_e for three wavelengths 443 nm, 636 nm, and 1550 nm were collected in the Supplementary Materials.

Both, deuterated structures nm_D and their hydrogen isotopologues nm_H showed close properties, when comparing homologues with the same number of carbon atoms. The differences in the values of refractive indices were very small, 0.001 on average, while it should be noted that the hydrogen structures nm_H had slightly higher values of refractive indices n_o and n_e . Therefore, minimum values differences were perceived in birefringence Δn (0.001 average)—See Figure 4.

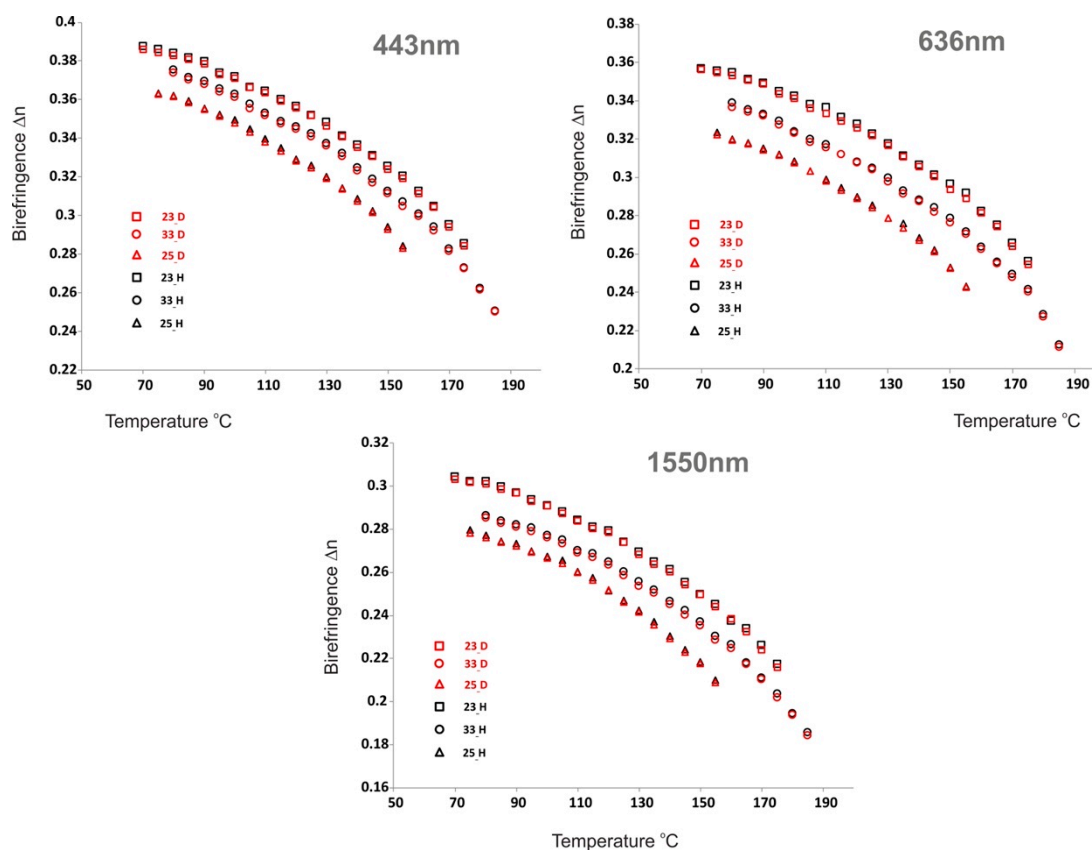


Figure 4. Temperature dependence of birefringence measured for 23_H, 33_H, 25_H, 23_D, 33_D, and 25_D at $\lambda = 443, 636,$ and 1550 nm.

2.4.1. Medium Wavelength Infrared MWIR Absorption (IR-C)—2500–17,000 nm (4000–600 cm^{-1}) Range

Measurements of infrared spectra using the transmittance FT-IR technique, with a carbon tetrachloride as solvent at a concentration of 0.1 M, were performed on the Nicolet iS10 Spectrometer Thermo Scientific (Thermo Fisher Scientific, Waltham, MA, USA). The spectra were measured in the range of 4000–1000 cm^{-1} with 32 scans and a resolution of 4 cm^{-1} . The windows in cuvette for testing the solutions were made of CaF_2 and the cuvette thickness was 0.5 mm. Before each sample measurement, a background measurement for pure solvent and air in the measuring chamber was recorded.

Regardless of the number of carbon atoms in terminal chain, FT-IR spectra of hydrogen compounds were very similar (see Figure 5). Bands at about 2970 cm^{-1} , 2870 cm^{-1} and 2930 cm^{-1} , 2850 cm^{-1} could be assigned to the asymmetric and symmetric stretching vibration between carbon and hydrogen atom in group CH_3 and CH_2 , respectively. Bands just above 3000 cm^{-1} were associated with stretching vibrations between carbon and hydrogen atoms in benzene rings. Bands at about 2210 cm^{-1} were connected with the stretching vibration of triple bonds between carbon atoms. Bands at about 1900 cm^{-1} could be assigned to the vibration of benzene rings. Bending vibration of functional groups inside studied compounds were visible as bands below 1700 cm^{-1} . As expected, the biggest difference in FT-IR spectra of deuterated isotopologues was the shift of bands from stretching C-H vibrations in aliphatic chains, toward lower wavenumber values (between 2220–2050 cm^{-1}). Due to the non-100% deuterium introduction efficiency in the aliphatic chains, a small band at around 2930 cm^{-1} was also observed. Nevertheless, the transmittance in the region between 3000–2500 cm^{-1} was above 80% for the compound 25_D, as well as 35_D, and was found to be much higher than in its hydrogen counterparts, 25_H and 35_H. It showed the potential advantage of studied deuterated compounds in

near-infrared applications where overtones of stretching vibrations in aliphatic chains were undesirable.

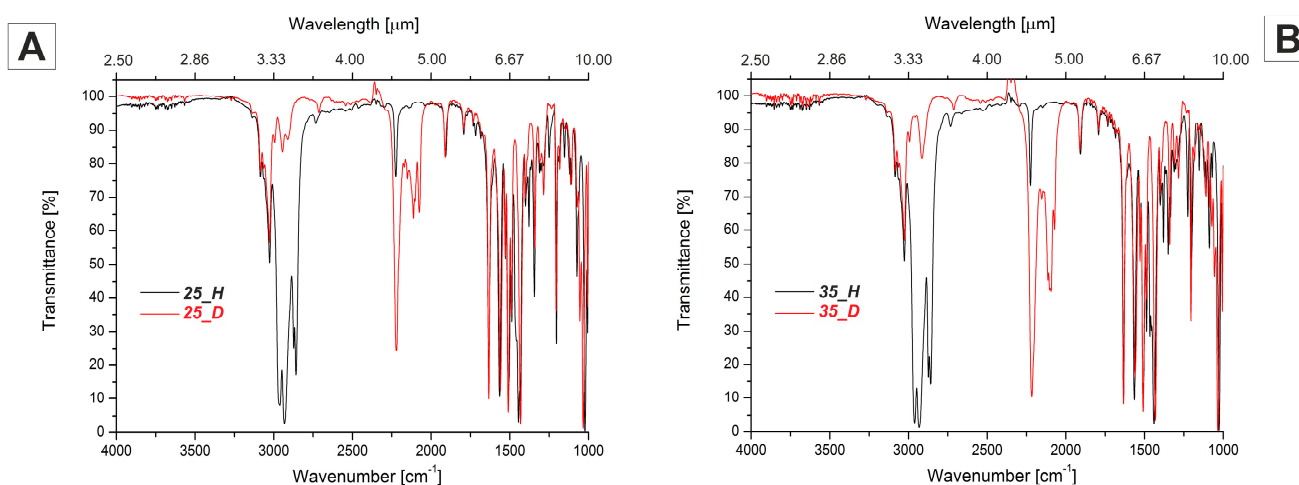


Figure 5. FT-IR spectra of selected isotopologues: (A) 25_H and 25_D , and (B) 35_H and 35_D .

2.4.2. Near-Infrared NIR Absorption (IR-A + IR-B)—800–2000 nm ($12,500$ – 5000 cm^{-1}) Range

The study of spectral characteristics in the near-infrared range (800–2000 nm) was carried out using the Shimadzu UV-Vis-NIR 3600 spectrophotometer (Shimadzu, Kyoto, Japan) using the transmission technique, in solutions. In transmission techniques, the oscillation spectrum was received by measuring the intensity of the radiation after it passed through the sample, where a decrease in the intensity of the incident beam indicated the absorption of the radiation. The spectrophotometer was equipped with three detectors, two of them were used to conduct measurements in the near-infrared range: indium–germanium–arsenic photodiode (InGaAs) and a cooled lead sulphide detector. The solutions of the tested compounds were prepared at concentrations of 0.5 M. Carbon tetrachloride was used as a solvent and spectra were recorded in quartz cuvettes with a volume of 1 mL with an optical path equal to 1 cm, made of black glass eliminating the phenomenon of internal reflection.

The overtones of C-H bond vibrations occurred at a frequency approximately two or three times higher than the fundamental vibration and were approximately forty to two hundred times weaker. They had similar patterns to those in the MWIR, although there were some differences, primarily a wider separation with each overtone, caused by minimalization of symmetric vibrations, leaving the asymmetric bands more isolated. The consolidated spectrum of alkyl-deuterated tolanes nm_D clearly showed the major peak at 1670 nm, which was assigned to the first overtone of the aromatic C-H stretch and was a doublet representing a combination of four individual fundamental bands, only one of which was IR active. The second overtone of C-H stretching vibrations was measured at 1135 nm—Figure 6. The non-deuterated isotopologues, nm_H , had additional absorption bands derived from C-H stretching vibrations in the aliphatic chain. The first overtones of C-H stretching occurred between 1680 and 1800 nm and the second overtones between 1150 and 1220 nm, where absorption bands of the methyl, methylene and methine groups occurred at different wavelengths. The first overtone of CH_3 asymmetrical and symmetrical stretches occurred at 1692 and 1700 nm, respectively. The asymmetric and symmetric CH_2 stretching bands appeared at approximately 1720 and 1760 nm, respectively. In the area of the second overtone, absorption was observed at 1185 nm and 1200 nm, corresponding to the vibrations in the CH_3 and CH_2 groups. The region of 1350–1430 nm was assigned as C-H combination bands: $2 \times \text{CH}$ stretch and CH bending of both CH_2 and CH_3 groups in the aliphatic chain.

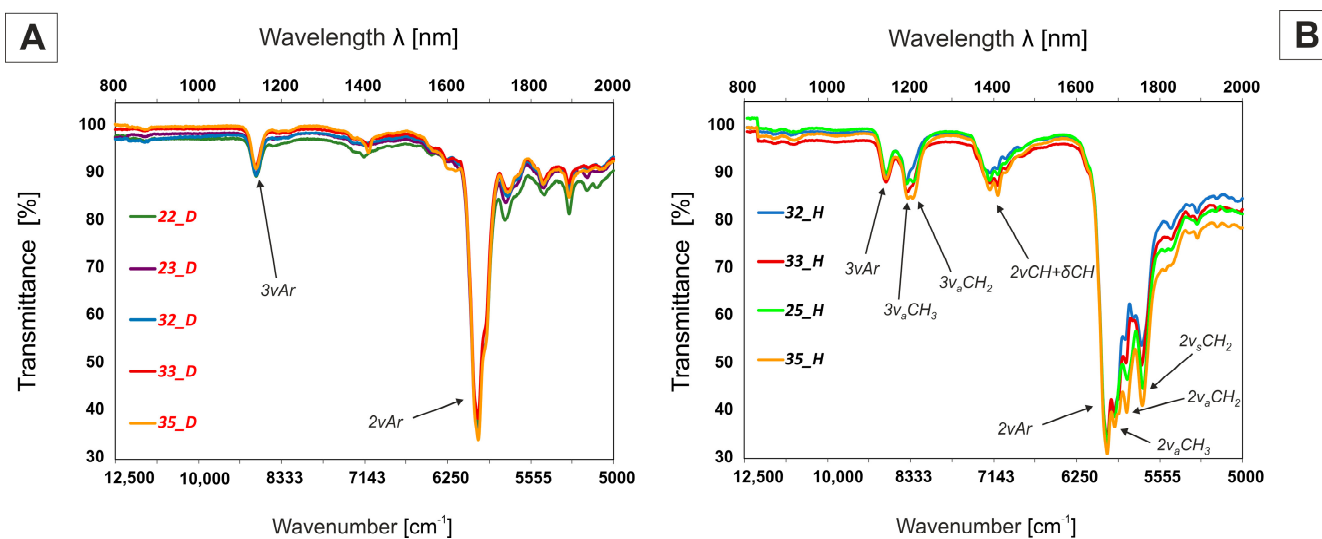


Figure 6. NIR spectra of deuterated compounds nm_D (A) and their hydrogen isotopologues nm_H (B) ($c = 0.5$ M), with ν -stretching vibrations, ν_a -asymmetric stretching, ν_s -symmetric stretching, and δ -bending vibrations.

3. Conclusions

In this work we showed the synthetic methodology, mesomorphic behavior and IR properties of deuterated versions of known nematics from the phenyltolane family. In the synthesis process, the main emphasis was placed on the use of the continuous flow reactor, where deuterated parts of molecules were formed. Isotopic pure-alkyl parts of molecules were created using the D-hydrogenolysis procedure of D_2 gas to CC triple bonds. The synthesis approach was successfully designed to minimize the number of deuterium sources and to rely as much as possible or solely on heavy water, which was the cheapest and most accessible deuterium source. Deuterated versions of liquid crystals showed almost identical properties to their hydrogen analogues both from the mesomorphic and optical (refractive indices) point of view. Of course, there were slight differences in the temperatures of phase transitions and the values of refractive indices, but these structures could still be twin-classified—at least from the mesomorphic and optical point of view. This should be considered as an advantage, since it was possible to predict the properties of deuterated structures without the need to synthetically obtain them. The cost of obtaining deuterated structures was much higher compared to the production of their hydrogen equivalents. The differences in properties that were clearly visible for this type of material could only be detected in the absorption of IR radiation. The deuterated versions of the liquid crystals that were investigated in this work showed significantly reduced absorption especially in the NIR range. This was the advantage of deuterated materials over hydrogen equivalents, especially when it came to the specific applications of liquid crystals beyond the visible spectrum.

Supplementary Materials: The following are available online at <https://www.mdpi.com/article/10.3390/ma14164653/s1>, Figure S1: DSC spectrum of compound 22_D, Figure S2: DSC spectrum of compound 22_H, Figure S3: DSC spectrum of compound 23_D, Figure S4: DSC spectrum of compound 23_H, Figure S5: DSC spectrum of compound 25_D, Figure S6: DSC spectrum of compound 25_H, Figure S7: DSC spectrum of compound 32_D, Figure S8: DSC spectrum of compound 32_H, Figure S9: DSC spectrum of compound 33_D, Figure S10: DSC spectrum of compound 33_H, Figure S11: DSC spectrum of compound 35_D, Figure S12: DSC spectrum of compound 35_H, Figure S13: MS spectrum of compounds 22_H and 22_D, Figure S14: MS spectrum of compounds 23_H and 23_D, Figure S15: MS spectrum of compounds 25_H and 25_D, Figure S16: MS spectrum of compounds 32_H and 32_D, Figure S17: MS spectrum of compounds 33_H and 33_D, Figure S18: MS spectrum of compounds 35_H and 35_D, Figure S19: IR spectrum of compound 22_H, Figure S20: IR spectrum of compound 22_D, Figure S21: IR spectrum of compound 23_H, Figure S22: IR spec-

trum of compound 23_D, Figure S23. IR spectrum of compound 25_H, Figure S24. IR spectrum of compound 25_D, Figure S25. IR spectrum of compound 32_H, Figure S26. IR spectrum of compound 32_D, Figure S27. IR spectrum of compound 35_H, Figure S28. IR spectrum of compound 35_D, Figure S29. ¹H NMR spectrum of compound 22_D, Figure S30. ¹H NMR spectrum of compound 23_D, Figure S31. ¹H NMR spectrum of compound 32_D, Figure S32. ¹H NMR spectrum of compound 33_D, Figure S33. ¹H NMR spectrum of compound 35_D, Figure S34. POM texture of nematic phase of compound 33_D, Figure S35. POM texture of nematic phase of compound 33_D, Figure S36. POM texture of nematic phase of compound 25_D, Figure S37. POM texture of nematic phase of compound 35_D, Table S1. Measured refractive indices (n_e and n_o) of 33_D at $\lambda = 443, 636,$ and 1550 nm, and at different temperatures, Table S2. Measured refractive indices (n_e and n_o) of 33_H at $\lambda = 443, 636,$ and 1550 nm, and at different temperatures, Table S3. Measured refractive indices (n_e and n_o) of 23_D at $\lambda = 443, 636,$ and 1550 nm, and at different temperatures, Table S4. Measured refractive indices (n_e and n_o) of 23_H at $\lambda = 443, 636,$ and 1550 nm, and at different temperatures, Table S5. Measured refractive indices (n_e and n_o) of 25_D at $\lambda = 443, 636,$ and 1550 nm, and at different temperatures, Table S6. Measured refractive indices (n_e and n_o) of 25_H at $\lambda = 443, 636,$ and 1550 nm, and at different temperatures.

Author Contributions: J.H., conceptualization, synthesis, measurements, methodology, writing and editing; P.H., synthesis, writing, editing; M.C. and O.S., measurements; M.P., synthesis; M.Z. instrumental analysis; P.K., synthesis. All authors have read and agreed to the published version of the manuscript.

Funding: This work was done with financial support from the of The National Centre for Research and Development grant DOB-1P/01/03/2016.

Institutional Review Board Statement: Not applicable.

Informed Consent Statement: Not applicable.

Data Availability Statement: Data are contained within the article or supplementary materials.

Conflicts of Interest: The authors declare no conflict of interest.

References

1. Pandey, K.K.; Tripathi, P.K.; Misra, A.K.; Manohar, R. UV response on dielectric properties of nano nematic liquid crystal. *Results Phys.* **2018**, *8*, 1119–1123. [[CrossRef](#)]
2. Li, Q.R.; Qiu, J.; Liu, H.G.; Chen, X. A luminescent lyotropic liquid crystal with UV irradiation induced photochromism. *Soft Matter* **2020**, *16*, 1170–1178. [[CrossRef](#)]
3. Chen, R.; An, Z.; Wang, W.; Chen, X.; Chen, P. Improving UV stability of tolane-liquid crystals in photonic applications by the ortho fluorine substitution. *Opt. Mater. Express* **2016**, *6*, 97–105. [[CrossRef](#)]
4. Pandey, K.K.; Dixit, A.C.; Khan, M.S.; Tripathi, P.K.; Misra, A.K.; Manohar, R. Effect of UV light irradiation on the dielectric behaviour of liquid crystal/nano composite. *Mol. Cryst. Liq. Cryst.* **2017**, *656*, 89–95. [[CrossRef](#)]
5. Wu, P.-C.; Yang, S.-Y.; Lee, W. Recovery of UV-degraded electrical properties of nematic liquid crystals doped with TiO₂ nanoparticles. *J. Mol. Liq.* **2016**, *218*, 150–155. [[CrossRef](#)]
6. Wang, Z.; Xu, T.; Noel, A.; Chen, Y.-C.; Liu, T. Applications of liquid crystals in biosensing. *Soft Matter* **2021**, *17*, 4675–4702. [[CrossRef](#)] [[PubMed](#)]
7. Beeckman, J.; Neyts, K.; Vanbrabant, P. Liquid-crystal photonic applications. *Opt. Eng.* **2011**, *50*. [[CrossRef](#)]
8. Harmata, P.; Herman, J. New-Generation Liquid Crystal Materials for Application in Infrared Region. *Materials* **2021**, *14*, 2616. [[CrossRef](#)]
9. Harmata, P.; Herman, J.; Kula, P. Liquid crystals for IR: Part I—synthesis and properties of perfluoroalkyl or perfluoroalkoxy terminated oligophenyls. *Liq. Cryst.* **2020**, *47*, 2122–2143. [[CrossRef](#)]
10. Harmata, P.; Herman, J.; Kula, P. Liquid crystals for IR: Part II synthesis and properties of perfluoroalkyl- or perfluoroalkoxy-terminated tolanes. *Liq. Cryst.* **2020**, *47*, 2144–2160. [[CrossRef](#)]
11. Kula, P.; Czerwiński, M.; Herman, J.; Harmata, P. Liquid Crystals for IR: Part III—Bi- and multicomponent mixtures based on perfluoroalkyl or perfluoroalkoxy terminated oligophenyls and tolanes. *Liq. Cryst.* **2020**, *47*, 2161–2170. [[CrossRef](#)]
12. Saito, M.; Hayashi, K. Integration of liquid crystal elements for creating an infrared Lyot filter. *Opt. Express* **2013**, *21*, 11984–11993. [[CrossRef](#)]
13. Zhang, Y.; Song, P.; Xia, W.; Wang, J.; Zhou, C.; Zhang, H. A low-loss and high birefringence fluoride photonic crystal fiber in near infrared band. *Optik* **2019**, *185*, 772–776. [[CrossRef](#)]
14. Kula, P.; Bennis, N.; Marć, P.; Harmata, P.; Gacjoch, K.; Morawiak, P.; Jaroszewicz, L.R. Perdeuterated liquid crystals for near infrared applications. *Opt. Mater.* **2016**, *60*, 209–213. [[CrossRef](#)]

15. Lu, H.B.; Xing, J.; Wei, C.; Sha, J.Q.; Zhang, G.B.; Lv, G.Q.; Zhu, J.; Qiu, L.Z. Near-infrared light directed reflection in a cholesteric liquid crystal. *Opt. Mater. Express* **2017**, *7*, 4163–4170. [[CrossRef](#)]
16. Nayak, R.A.; Veerabhadraswamy, B.N.; Shankar Rao, D.S.; Sudhakar, A.A.; Yelamaggad, C.V. Room-Temperature, Deep-Red/NIR-Emissive, C₃-Symmetric (n, π -conjugated) Columnar Liquid Crystals: C₃h-Tris(keto-hydrazone)s. *ACS Omega* **2021**, *6*, 3291–3306. [[CrossRef](#)]
17. Hacker, E.; Lauth, H.; Reichel, F. Optically addressable liquid-crystal spatial light modulators for VIS to NIR light modulation. *SPIE* **1998**, *3292*, 13–24.
18. Sun, C.; Lu, J. A Tunable NIR Filter with Sphere Phase Liquid Crystal. *Crystals* **2019**, *9*, 349. [[CrossRef](#)]
19. Liu, W.; Guo, L.-X.; Lin, B.-P.; Zhang, X.-Q.; Sun, Y.; Yang, H. Near-Infrared Responsive Liquid Crystalline Elastomers Containing Photothermal Conjugated Polymers. *Macromolecules* **2016**, *49*, 4023–4030. [[CrossRef](#)]
20. Kang, B.; Woo, J.H.; Choi, E.; Lee, H.-H.; Kim, E.S.; Kim, J.; Hwang, T.-J.; Park, Y.-S.; Kim, D.H.; Wu, J.W. Optical switching of near infrared light transmission in metamaterial-liquid crystal cell structure. *Opt. Express* **2010**, *18*, 16492–16498. [[CrossRef](#)]
21. Bortolozzo, U.; Residori, S.; Huignard, J.-P. Transmissive liquid crystal light-valve for near-infrared applications. *Appl. Opt.* **2013**, *52*, E73–E77. [[CrossRef](#)]
22. Wu, S.T. Infrared Properties of Nematic Liquid-Crystals—An Overview. *Opt. Eng.* **1987**, *26*, 120–128. [[CrossRef](#)]
23. Wu, S.-T.; Cox, R.J. Potential infrared liquid crystals. *Liq. Cryst.* **1989**, *5*, 1415–1424. [[CrossRef](#)]
24. Wu, S.-T.; Wang, Q.-H.; Kempe, M.D.; Kornfield, J.A. Perdeuterated cyanobiphenyl liquid crystals for infrared applications. *J. Appl. Phys.* **2002**, *92*, 7146–7148. [[CrossRef](#)]
25. Lipiński, K.; Lipiński, T.; Chruściel, J.; Suszko-purzycka, A.; Rykowski, A. Synthesis and Mesomorphic Properties of Deuterated 4-n-Pentylphenyl-4'-n-Alkoxythiobenzoates 7S5-d26 and 8S5-d28. *Mol. Cryst. Liq. Cryst. Sci. Technol. Sect. A. Mol. Cryst. Liq. Cryst.* **1994**, *239*, 87–93. [[CrossRef](#)]
26. Kula, P.; Herman, J.; Harmata, P.; Czerwiński, M. NIR and MWIR transparent liquid crystals. In Proceedings of the 2014 39th International Conference on Infrared, Millimeter, and Terahertz waves (IRMMW-THz), Tucson, AZ, USA, 14–19 September 2014.
27. Gray, G.W.; Mosley, A. The Synthesis of Deuterated 4-n-Alkyl-4'-Cyanobiphenyls. *Mol. Cryst. Liq. Cryst.* **1978**, *48*, 233–242. [[CrossRef](#)]
28. Dong, R.Y. Recent NMR Studies of Thermotropic Liquid Crystals. *Annu. Rep. NMR Spectrosc.* **2016**, *87*, 41–174. [[CrossRef](#)]
29. Chen, Y.; Xianyu, H.; Sun, J.; Kula, P.; Dabrowski, R.; Tripathi, S.; Twieg, R.; Wu, S.-T. Low absorption liquid crystals for mid-wave infrared applications. *Opt. Express* **2011**, *19*, 10843–10848. [[CrossRef](#)]
30. Hu, M.; An, Z.; Li, J.; Chen, H.; Peng, F.; Wu, S.-T.; Wang, X.; Li, M. Low mid-infrared absorption tolane liquid crystals terminated by 2,2-difluorovinyl: Synthesis, characterization and properties. *J. Mater. Chem. C* **2016**, *4*, 4939–4945. [[CrossRef](#)]
31. Hu, M.; An, Z.; Li, J.; Mo, L.; Yang, Z.; Li, J.; Che, Z.; Yang, X. Tolane liquid crystals bearing fluorinated terminal group and their mid-wave infrared properties. *Liq. Cryst.* **2014**, *41*, 1696–1702. [[CrossRef](#)]
32. Peng, F.; Lee, Y.-H.; Chen, H.; Li, Z.; Bostwick, A.E.; Twieg, R.J.; Wu, S.-T. Low absorption chlorinated liquid crystals for infrared applications. *Opt. Mater. Express* **2015**, *5*, 1281–1288. [[CrossRef](#)]
33. Gu, D.; Wen, B.; Mahajan, M.; Taber, D.; Winker, B.; Guthals, D.; Campbell, B.; Sox, D. High power liquid crystal spatial light modulators. *SPIE* **2006**, *9*, 427.
34. Schmid, A.; Papernov, S.; Zheng, W.; Marshall, K.; Gunderman, T.; Lee, J.-C.; Guardalben, M.; Jacobs, S.D. Liquid-Crystal Materials for High Peak-Power Laser Applications. *Mol. Cryst. Liq. Cryst.* **1991**, *207*, 33–42. [[CrossRef](#)]
35. Zhuang, Z.; Suh, S.-W.; Patel, J.S. Polarization controller using nematic liquid crystals. *Opt. Lett.* **1999**, *24*, 694–696. [[CrossRef](#)]
36. Aharon, O.; Abdulhalim, I. Liquid crystal wavelength-independent continuous polarization rotator. *Opt. Eng.* **2010**, *49*, 034002. [[CrossRef](#)]
37. Tani, T.; Shribak, M.; Oldenbourg, R. Living Cells and Dynamic Molecules Observed with the Polarized Light Microscope: The Legacy of Shinya Inoué. *Biol. Bull.* **2016**, *231*, 85–95. [[CrossRef](#)] [[PubMed](#)]
38. Koike-Tani, M.; Tominaga, T.; Oldenbourg, R.; Tani, T. Instantaneous polarized light imaging reveals activity dependent structural changes of dendrites in mouse hippocampal slices. *bioRxiv* **2019**, 523571. [[CrossRef](#)]
39. Abdulhalim, I. Non-display bio-optic applications of liquid crystals. *Liq. Cryst. Today* **2011**, *20*, 44–60. [[CrossRef](#)]
40. Sattar, S.; Lapray, P.; Foulonneau, A.; Bigué, L. Review of spectral and polarization imaging systems. In Proceedings of the SPIE Photonics Europe, Strasbourg, France, 6 April 2020.
41. Abdlaty, R.; Sahli, S.; Hayward, J.; Fang, Q. Hyperspectral imaging: Comparison of acousto-optic and liquid crystal tunable filters. *SPIE* **2018**, *10573*, 105732P.
42. Wang, W.; Li, C.; Tollner, E.W.; Rains, G.C.; Gitaitis, R.D. A liquid crystal tunable filter based shortwave infrared spectral imaging system: Design and integration. *Comput. Electron. Agric.* **2012**, *80*, 126–134. [[CrossRef](#)]
43. Messaadi, A.; Sánchez-López, M.d.M.; García-Martínez, P.; Vargas, A.; Moreno, I. Optical system for measuring the spectral retardance function in an extended range. *J. Eur. Opt. Soc.-Rapid Publ.* **2016**, *12*, 21. [[CrossRef](#)]
44. Sordillo, L.; Pu, Y.; Pratavieira, S.; Budansky, Y.; Alfano, R. Deep optical imaging of tissue using the second and third near-infrared spectral windows. *J. Biomed. Opt.* **2014**, *19*, 056004. [[CrossRef](#)]
45. García-Martínez, P.; Moreno, I.; Sánchez-López, M.d.M.; Gomis, J.; Martínez, P.; Cofré, A. Programmable Supercontinuum Laser Spectrum Generator Based on a Liquid-Crystal on Silicon Spatial Light Modulator. *Front. Phys.* **2021**, *9*. [[CrossRef](#)]

46. Moreno, I.; Carrión, J.V.; Martínez, J.L.; García-Martínez, P.; Sánchez-López, M.M.; Campos, J. Optical retarder system with programmable spectral retardance. *Opt. Lett.* **2014**, *39*, 5483–5486. [[CrossRef](#)]
47. Lee, Y.U.; Kim, J.; Wu, J.W. Electro-optic switching in metamaterial by liquid crystal. *Nano Converg.* **2015**, *2*, 23. [[CrossRef](#)]
48. Herman, J.; Harmata, P.; Strzeżysz, O.; Czerwiński, M.; Urban, S.; Kula, P. Synthesis and properties of chosen 4-butyl-phenyltolane derivatives—On the influence of core substitution on birefringence, mesomorphic and dielectric properties. *J. Mol. Liq.* **2018**, *267*, 511–519. [[CrossRef](#)]
49. Kula, P.; Aptacy, A.; Herman, J.; Wojciak, W.; Urban, S. The synthesis and properties of fluoro-substituted analogues of 4-butyl-4'-[(4-butylphenyl)ethynyl]biphenyls. *Liq. Cryst.* **2013**, *40*, 482–491. [[CrossRef](#)]
50. Buchecker, R.; Marck, G.; Schadt, M. New Nematics Incorporating a 2,6-Difluorophenyl Acetylene Group. *Mol. Cryst. Liq. Cryst. Sci. Technol. Sect. A. Mol. Cryst. Liq. Cryst.* **1995**, *260*, 93–105. [[CrossRef](#)]
51. Seils, F.; Schadt, M. Liquid Crystals with a Chlorovinyl Side Chain; Effect of Structural Variations on the Dielectric Anisotropy. *Mol. Cryst. Liq. Cryst. Sci. Technol. Sect. A. Mol. Cryst. Liq. Cryst.* **1995**, *260*, 127–138. [[CrossRef](#)]
52. Herman, J.; Kula, P. The synthesis of chiral fluorinated 4-alkyl-4'-[(4-alkylphenyl)ethynyl]biphenyls. *Tetrahedron Lett.* **2013**, *54*, 3621–3623. [[CrossRef](#)]